Nanostructured Coatings by Adhesion of Phosphonated Polystyrene Particles onto Titanium Surface for Implant Material Applications

Anke Zeller,[†,‡] Anna Musyanovych,*[,†,‡] Michael Kappl,[†] Anitha Ethirajan,[†] Martin Dass,[†] Dilyana Markova,[†] Markus Klapper,[†] and Katharina Landfester[†,‡]

Max Planck Institute for Polymer Research, Ackermannweg 10, 55128 Mainz, Germany, and Institute of Organic Chemistry III—Macromolecular Chemistry and Organic Materials, University of Ulm, Albert-Einstein-Allee 11, 89081 Ulm, Germany

ABSTRACT Titanium that is covered with a native oxide layer is widely used as an implant material; however, it is only passively incorporated in the human bone. To increase the implant—bone interaction, one can graft multifunctional phosphonic compounds onto the implant material. Phosphonate groups show excellent adhesion properties onto metal oxide surfaces such as titanium dioxide, and therefore, they can be used as anchor groups. Here, we present an alternative coating material composed of phosphonate surface-functionalized polystyrene nanoparticles synthesized via free radical copolymerization in a direct (oil-in-water) miniemulsion process. Two types of functional monomers, namely, vinylphosphonic acid (VPA) and vinylbenzyl phosphonic acid (VBPA), were employed in the copolymerization reaction. Using VBPA as a comonomer leads to particles with a higher density of surface phosphonate groups in comparison to those obtained with VPA. VBPA-functionalized particles were used for the coating formation on the titanium surface. The particles monolayer was investigated by scanning electron microscopy (SEM) and atomic force microscopy (AFM) employing titanium and silicium tip with the native OH groups. Force versus distance curves proves the strong adhesion between the phosphonated particles and the titanium (or silicium) surfaces in contrast to the nonfunctionalized polystyrene particles. Finally, as a proof of concept, the particles adhered to the surface were further used to nucleate hydroxyapatite, which has high potential for bioimplants.

KEYWORDS: functional particles • phosphonate groups • titanium coating • atomic force microscopy • mineralization

INTRODUCTION

Creation of a thin layer to promote the adhesion on to metal surfaces plays an important role in various fields of application. In particular, the corrosion inhibition (1, 2) or the modification of implant materials in order to get the protein resistant surfaces (3—9) is of great interest. To achieve an effective adhesion promotion for different surfaces, specific anchor groups are necessary. Phosphonate groups are typical anchor groups for metals such as titanium, aluminum, tantalum, etc., which are covered with a native oxide layer bearing hydroxyl groups on the metal surface (10—14). Therefore, it is the oxide layer which is the effective binding surface. Phosphonic acid grafts to the metal oxide surface via strong acid/base interactions (1, 15). In fact, different bonding modes can be formed. For titanium/titanium oxide surfaces, the formation of monodentate, bidentate or tridentates is possible (16, 17). A tridentate, for example, is formed between two ester bonds of the phosphonate groups and surface OH groups, while the P═O group is attached through a hydrogen bond (1). The bond formation of phosphonate groups onto the titanium oxide surfaces was studied in detail by Park et al. (15) The authors used phosphonate groups as anchor for Ru-bipyridyl complexes onto titanium oxide surfaces in TiO_2 solar cells. Based on the high affinity of phosphonate groups to metal ions like Cu(II), Co(II), Ag(I), Ni(II) and Cr(III) under controlled pH value, functionalized water-soluble polymers were used as binders to recover the metal ions from dilute solution such as wastewater or industrial fluids (18). Several research groups have been intensively studied the formation and stability/dynamics of the self-assembled monolayers (SAMs) using the alkyls molecules with the end-functionalized phosphonate as an anchor group for the metal oxide surface (10—14, 19, 20).

Few papers describe the application of polymeric nanoparticles having phosphonate groups on the surface. Henke et al. (2) used the phosphate functionalized well-packed microgels as the corrosion protective layers for reactive metal surfaces. Titanium is used for hard tissue replacement due to its high chemical stability in the body (21). To increase the chemical interaction between the implant and bone tissue, several phosphonic acid compounds (e.g., methylenediphosphonic acid, propane-1,1,3,3 tetraphosphonic acid) have been described in the literature (21). Here we show an alternative implant coating material based on the phospho-

* Corresponding author. E-mail: musyanovych@mpip-mainz.mpg.de. Tel: +49(0)6131 379-248. Fax: +49(0)6131 379-100.
Received for review May 16, 2010 and accepted July 14, 2010
† Max Planck Institute for Polymer Research.
‡ University of Ulm.
DOI: 10.1021/am1004305

nate surface-functionalized polymeric nanoparticles. The particles were prepared by miniemulsion polymerization, which is an efficient method to obtain nanoparticles with different surface functionalities, controlled particle size and size distribution (22−24). The main advantage of the polymeric coating materials is the high amount of phosphonate groups at the particle surface. On the one hand, the surface phosphonate groups can serve as anchor groups to the implant material. On the other hand, the high amounts of excessive groups can be used to nucleate hydroxyapatite, which can support the interaction to the bone tissue. Previously, surface-functionalized particles with different amount of carboxyl groups were successfully used to study the nucleation of hydroxyapatite (25). Polystyrene as a material of nanoparticles is only a model system for particle based functionalization. It can be replaced by suitable biodegradable material and applied in the release of therapeutics.

In this current work, the synthesis and properties of vinylbenzyl phosphonic acid (VBPA)-functionalized particles were compared with the particles obtained in the presence of vinylphosphonic acid (VPA). In our recent publication, the synthesis of VPA functionalized polystyrene and poly(methyl methacrylate) based nanoparticles was described in detail (24). The main difference between VPA and VBPA is the solubility: VPA is completely water-soluble, whereas VBPA is an oil-soluble monomer containing ionic groups. It is known that the solubility influences the participation of the monomer in the copolymerization reaction as well as its incorporation into the polymeric chain and distribution on the final particle surface. The particles were characterized in terms of average size, polydispersity, surface groups' density, and morphology. The obtained phosphonate functionalized particles were used to form particle layer onto titanium and silicon surfaces. The particle layer formation on the substrates was studied by scanning electron microscopy (SEM). Force distance curves, measured with atomic force microscopy (AFM), were used to study the adhesion forces of the phosphonate-functionalized and nonfunctionalized polystyrene particles. As a proof of concept, functionalized particles adhered to the surface were further used to nucleate calcium phosphate, which has high potential for bioimplants.

EXPERIMENTAL SECTION

Materials. Styrene (Merck) was freshly distilled under reduced pressure before use. Vinylphosphonic acid (VPA) (Aldrich, 97%) was washed with diethyl ether and dried under vacuum to remove an inhibitor. All other reagents and solvents were commercial products and were used without further purification: the hydrophobe, i.e., hexadecane (Aldrich, 99%); the hydrophobic initiator 2,2′-azobis(2-methylbutyronitrile) (V59) from Wako Chemicals, Japan; the surfactant Lutensol AT50, which is a poly(ethylene oxide)-hexadecyl ether with an EO block length of about 50 units, was supplied from BASF. For the loading of the particles, calcium nitrate tetrahydrate (Aldrich, 99%), diammonium hydrogen phosphate (Merck), and 28% ammonia solution (VWR) were used. Demineralized water was used during the experiments.

Synthesis of Phosphonate Functionalized Polymer Nanoparticles by Miniemulsion Process. The phosphonate surface-functionalized polystyrene particles were synthesized by a free-radical copolymerization of styrene and with either vinylphosphonic acid (VPA) (polySt−polyVPA) or vinylbenzylphosphonic acid (VBPA) (polySt−polyVBPA) in a miniemulsion process. The chemical structures of VPA and VBPA are presented in Figure 1. The monomer VBPA was synthesized applying following procedure. The precursor monomer diethyl *p*-vinylbenzylphosphonate (DEVBP) was synthesized according to ref 26. The obtained product was purified by column chromatography on silica, eluting first the unreacted vinylbenzyl chloride with CH_2Cl_2 and then changing to ethyl acetate for the elution of DEVBP. This monomer was further deprotected using the bromotrimethylsilane (TMSBr)/methanolysis approach. Typically, the phosphonate was reacted with a 5-fold molar excess of TMSBr (related to the phosphonate groups amount) in CH_2Cl_2 (5% solution) at room temperature for 24 h. After evaporation of the volatiles, the silylated ester was reacted with a large excess of methanol at room temperature for 24 h. The VBPA was obtained in quantitative yield after the evaporation of the solvent under reduced pressure and drying in vacuum at room temperature for at least 12 h.

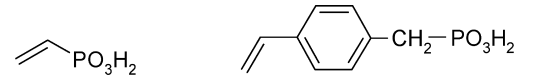

Vinylphosphonic acid (VPA) Vinylbenzylphosphonic acid (VBPA)

FIGURE 1. Chemical structure of the used phosphonated comonomers.

For the synthesis of polySt−polyVBPA latex particles, a given amount of styrene (varied between 6 and 5.4 g), VBPA (varied between 0 and 0.6 g), 250 mg of hexadecane, and 100 mg of initiator V59 were mixed together and emulsified in 24 g water containing 200 mg of the nonionic surfactant Lutensol AT50. After 1 h of stirring at 1000 rpm the miniemulsion was prepared by ultrasonication for 120 s at 90% intensity (Branson sonifier W450 Digital, 1/2 in. tip) at 0 °C in order to prevent polymerization of the monomer(s). Afterward, the miniemulsion was transferred into a round-bottom flask and polymerization was carried out at 72 °C under stirring overnight. The synthesis of polySt−polyVPA latex particles was performed with the same amount of the reagents and in a same manner as polySt−polyVBPA, with the exception that the functional monomer (VPA) was added into the aqueous phase.

Characterization of the Functionalized Polymer Particles. The average particle size and the polydispersity index (PDI) was determined by dynamic light scattering (DLS) using a Nicomp 380 Submicrometer Particle Sizer (Nicomp Particle Sizing Systems, USA) at 20 °C and a scattering angle of 90°. The solid content of the samples was determined gravimetrically. All samples were cleaned by repetitive centrifugation/redispersion in demineralized water. The zeta potential was measured in 1×10^{-3} M KCl with a Nicomp Zeta Sizer (Nicomp Particle Sizing Systems, USA) at 20 °C. The density of phosphonate groups on the particle surface was determined by titration against the opposite charged polyelectrolyte poly(diallyldimethyl ammonium chloride) (PDADMAC) using a particle charge detector (Mütek GmbH, Germany) in combination with a Titrino Automatic Titrator (Metrohm AG, Switzerland). For the measurement, 10 mL of the latex sample with a solid content of 1 g/L were used. The amounts of groups were calculated from the amount of consumed polyelectrolyte (23). The particle size and morphology were examined by transmission electron microscopy (Philips EM400) at an acceleration voltage of 80 kV. Analytical transmission electron microscopy was carried out to study the phosphorus distribution on the particles surface and inside the particles. The surface elemental analysis was performed on the dried particles (placed on the copper grid) using elemental specific imaging (ESI). For visualization of phosphorus

distribution throughout the particle, they were stained by 1% uranylacetate and 1% osmiumtetroxide for 1 h and embedded in EPON followed by ultramicrotomy. The obtained ultrathin sections (thickness of 60 nm) were analyzed by electron energy loss spectroscopy (EELS) and ESI in a Zeiss EM912 (Carl Zeiss, Oberkochen, Germany) using the Omega-type energy filter. The microscope was operated at 120 kV with a emission current of 23 μA, illumination angle of 1.6 mrad, and slit aperture of 40 eV. Phosphorus was detected at the L23 ionization edge with energy loss of 132 eV and image EELS series were detected between $\Delta E = 193 \pm 2$ eV and $\Delta E = 115 \pm 2$ eV. Data sets were calculated using the Olympus iTEM software 5.0. The energy dispersive X-ray (EDX) analysis was performed on TEM (Tecnai200, FEI, Eindhoven, Netherlands) operated at 200 kV. The particle layers were examined by scanning electron microscopy (Zeiss 1530 Gemini, Carl Zeiss AG, Oberkochen, Germany) at an acceleration voltage of 0.1 to 1 kV. The latexes were diluted in demineralised water and a drop of the dispersion was placed on a silica wafer coated with a 20 nm TiO_2 layer.

Analytical Methods of Particle Layer Characterization. For the adsorption experiments and the AFM measurements Si wafers sputtered with 20 nm TiO_2 were used. The Si wafer was cleaned with demineralised water, 25% ammonia solution, 35% hydrogen peroxide solution and followed by repetitive rinsing with demineralised water and ethanol. The particle monolayer was generated by drop casting onto the wafer. During the drop-casting process, the wafer was placed on a ramp (13° slope) to support the particle layer formation on the substrates. The particle monolayer formation was controlled by SEM and AFM. AFM imaging and force spectroscopy were carried out with a Dimension 3100 microscope (Veeco Instruments, Plainview, USA) equipped with Nanoscope V controller and software version 7.20, using the silicon cantilevers with a resonance frequency of 70 kHz and a nominal spring constant of 2 N/m (OMCL-AC240TS, Olympus, Tokyo, Japan). Spring constants of cantilevers were determined using the thermal noise method (27). Cantilevers with tips were pretreated in a plasma oven and either used directly or were sputter-coated with 20 nm TiO_2. To exclude the influence of the possible variation in AFM tip shape, we carried out comparative measurements on the different substrates using the same cantilever. Particle layers were imaged in tapping mode. To measure the interaction between AFM tips and particle surfaces, we zoomed in onto locations close to the crest of one particle. Cantilever deflection versus piezo position curves were recorded at several places on each particle and the resulting curves were converted to force versus distance curves (in the following called force curves) by subtracting cantilever deflection from piezo position and multiplying the cantilever deflection with the spring constant (28). The force necessary to pull the tip from the surface is the adhesion force. Both conversion of raw data to force versus distance curves and the calculation of the adhesion force were performed by self-written software.

Mineralization on the Particles Adsorbed on the Surface. The latex of functionalized particles (AZ-5VBPA) with 0.1% solid content was drop casted on to the titanium substrates. The particles were allowed to adhere onto the surface of the substrate. The substrates were then carefully washed to remove unbounded particles. This was performed by multiple immersions of the substrates in to a Petri dish filled with demineralized water followed by rinsing with a gentle stream of demineralized water. The washed substrate was carefully suspended via a holder in to the solution containing dissolved $Ca(NO_3)_2 \cdot 4H_2O$. The pH of the solution was adjusted to 10 by using dilute ammonia solution and the molar ratio of calcium to phosphate for the loading was kept at 5:3. The solution was gently stirred at 37 °C (like in our previous experiment (25)) to allow binding of calcium ions and then loaded with phosphate ions as follows. Initially, 1 mL of 0.005 M $Ca(NO_3)_2 \cdot 4\ H_20$ was added to 9 mL of demineralized water followed by immersing of the substrate with the holder in to this solution. After 2 h of gentle stirring of the solution to allow binding of calcium ions, 1 mL of 0.003 M $(NH_4)_2HPO_4$ was added dropwise for about 1 h. The samples were stirred after loading for about 24 h. The pH was maintained at pH 10 throughout the experiment. After 24 h the substrates were once again washed in the same way as mentioned before for further characterization by SEM.

Table 1. Characterization of Functionalized Particles

sample name	comonomer amount (wt %)[a]	D_z (nm)[b]	PDI	solid content (%)[c]	Zeta potential (mV)
AZ-0	0	210	0.02	19.8	−3
PolySt−PolyVBPA Particles					
AZ-1VBPA	1	267	0.03	19.7	−12
AZ-3VBPA	3	253	0.03	18.7	−30
AZ-5VBPA	5	240	0.02	20.0	−36
AZ-10VBPA	10	231	0.06	19.6	−40
PolySt−PolyVPA Particles					
AZ-1VPA	1	247	0.03	15.7	−11
AZ-3VPA	3	231	0.05	19.2	−15
AZ-5VPA	5	228	0.06	16.3	−16
AZ-10VPA	10	210	0.09	17.7	−19

[a] Related to the total monomer amount of 6 g. [b] Determined by DLS. [c] Determined gravimetrically.

RESULTS AND DISCUSSION

Synthesis and Characterization of Phosphonate Functionalized Polystyrene Particles. PolySt−polyVPA and polySt−polyVBPA copolymer particles were synthesized in the presence of 3.3 wt % nonionic surfactant Lutensol AT50. The oil soluble initiator V59 was used in order to form the radicals inside the monomer droplets. For suppression of the droplets degradation through Ostwald ripening, the ultrahydrophobe hexadecane was employed. To obtain particles with different amounts of phosphonate groups on the surface, the introduced amount of functional comonomer was varied in the range between 0 and 10 wt % (related to the total monomer amount of 6 g). The characterization of the obtained particles in terms of average particle diameter (D_z), polydispersity index (PDI), solid content, and zeta potential are summarized in Table 1.

From Table 1, it can be seen that the average diameter of functionalized particles decreases with increasing VBPA or VPA amounts. The decrease in particle size is due to the increase in the number of charged phosphonate groups that are covalently attached to the particle surface. This results in the additional electrostatic stabilization of the droplets during the polymerization process. VPA-functionalized particles are slightly smaller in size as compared to those functionalized with VBPA. This could be explained by surface-active properties of VPA (24). During the droplet formation it serves as additional surfactant, reducing the initial droplets size and after polymerization resulting in the smaller particle diameter. Nonfunctionalized particles are smaller or have the same size as 10 wt % VPA-functionalized particles.

Table 2. Surface Functional Groups Density as a Function of the Type and Introduced Amount of the Comonomer

polySt−polyVBPA			polySt−polyVPA		
sample name	D_z (nm)[a]	amount of $-PO_3H_2$ groups per nm^2	sample name	D_z (nm)[a]	amount of $-PO_3H_2$ groups per nm^2
AZ-0	210	0	(pure polystyrene particles)		
AZ-1VBPA	267	0.87	AZ-1VPA	247	0.10
AZ-3VBPA	253	1.49	AZ-3VPA	231	0.19
AZ-5VBPA	240	1.88	AZ-5VPA	228	0.25
AZ-10VBPA	231	2.09	AZ-10VPA	210	0.42

[a] Determined by DLS.

Although VPA as well as VBPA brings additional electrostatic stabilization to the droplets, the comonomer amounts introduced for copolymerization are not significant compared to the stabilizing properties of Lutensol AT50.

The polySt−polyVBPA particles are approximately 20 nm bigger in size than the polySt−polyVPA particles. This could be due to the differences in the hydrophilic properties of VBPA and VPA. As was previously shown, the use of hydrophobic monomers leads to larger particles caused by a larger interfacial tension between the monomer and the water phase, which has to be compensated by a higher coverage with surfactant molecules (29).

The polydispersity index (PDI) shows the uniformity in size of the particles. Generally, PDI values lower than 0.1 indicate monodisperse distribution of the particles. The obtained solid contents of the dispersions were in the range of 18.7 to 20.0% (theoretical value is 21.4%). The conversion of the monomer(s) was almost 100%. The zeta potential of pure polystyrene sample (AZ-0) has minor negative charge, which is a result of the hydroxyl-ion adsorption at the interface (30). A clear dependency of the zeta potential as a function of the introduced functional comonomer amount was observed for both phosphonated comonomers. The particles obtained in the presence of higher comonomer concentration possess more negative zeta potential values. These results were supported by determining the amount of surface phosphonate groups from the titration against the opposite charged polyelectrolyte, i.e., polyDADMAC. In Table 2, the numbers of functional groups at the particle surface for both types of comonomers are summarized.

It can be seen that the concentration of phosphonate groups increases with increasing VBPA or VPA comonomer amount. For both types of comonomer, the density of surface phosphonate groups is in the range between 0.1 and 2.09 groups per nm^2. Furthermore, the surface coverage is much higher in the case of using VBPA as a comonomer, although the molar ratio of VBPA to VPA is approximately 1:1.7. This could be explained by differences in the molecule structure. VBPA has a better affinity to the styrene because of the presence of the benzene ring in the chemical structure (Figure 1) and therefore, more hydrophobic character. After the formation of miniemulsion droplets, VBPA mainly stays inside or at the interface of the droplets. In contrast, VPA preferentially stays in the continuous phase. It has to diffuse through the water phase and the surfactant layer in order to catch the radicals and participate in the polymerization.

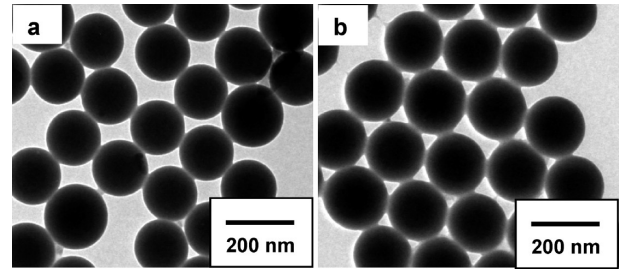

FIGURE 2. TEM images of (a) pure polystyrene particles (sample AZ-0) and (b) polySt−polyVBPA particles with 5 wt % VBPA (AZ-5VBPA).

The morphology of the particles was studied by TEM. As an example, the images of nonfunctionalized (AZ-0) and VBPA-functionalized particles (AZ-5VBPA) are shown in Figure 2. It can be seen that the particles are spherical in shape and homogeneous in size.

The composition of phosphonated particles was studied in detail by the electron energy loss spectroscopy (EELS) and element specific imaging (ESI) measurements (Figure 3). ESI images indicate a phosphorus distribution at the particle surface. However, the distribution of phosphorus inside the particles could not be detected on bulky particles because of the sample thickness. Therefore, the phosphorus distribution in ultrathin sections was analyzed as well. From the obtained images (Figure 4), a dark stained surface could be seen in the bright field, caused by the uranylacetate, which is a good staining agent for the phosphate groups (31). ESI performed at the ionization edge of phosphorus at 132 eV demonstrates the elemental mapping of the element. The obtained results revealed higher phosphorus content at the particle surface compared to the inner part of the particles. This is in agreement with the PCD results and confirms that the miniemulsion droplets interface is the main locus of VBPA and styrene copolymerization.

In addition, the EDX measurements were done as shown in Figure 5. Line scans through the particle indicates a higher concentration of phosphor at the particle surface and confirm the ESI results described above.

Determination of the Adhesion Forces by AFM. As described before, the polySt-polyVPA sample with 5 wt % of the VBPA comonomer amount (AZ-5VBPA) shows a narrow size distribution (PDI = 0.02) and possesses a high number of surface functional groups (1.88 phosphonate groups per nm^2). Therefore, this sample was used for the formation of the particle layer on metal (oxide) surfaces. Si wafer sputtered with 20 nm TiO_2 and the pure pretreated Si wafer, which bears a native hydroxyl-layer in presence of oxygen, were used as a substrate and placed on a ramp with 13° slope. The latex sample with a solid content of 1 g/L was deposited by the drop casting onto the substrate and dried overnight. In Figure 6, the SEM images of the resulting particle layer are shown.

From the SEM images, it can be clearly seen that the particles show high size uniformity. They form a densely packed monolayer on the metal oxide substrates with a

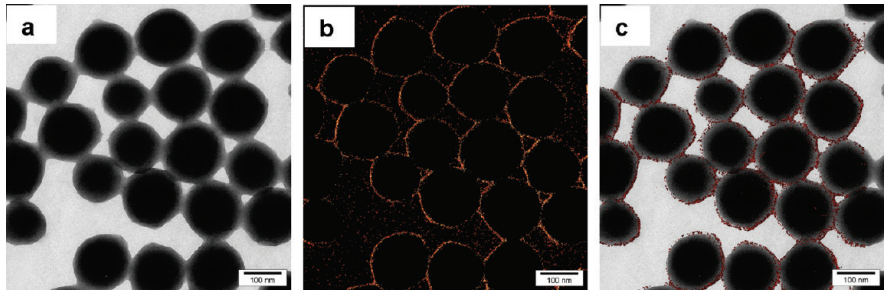

FIGURE 3. (a) Bright-field image of nonsectioned polystyrene particles with phosphonate groups (AZ-5VBPA). (b) ESI image of phosphorus distribution at the same position as shown in image a. (c) Combination of the images a and b.

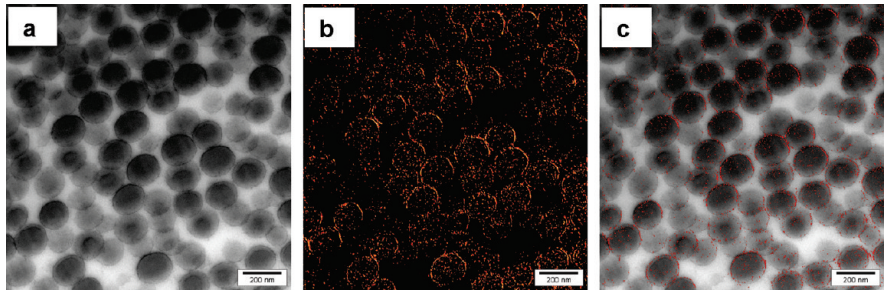

FIGURE 4. (a) Ultrathin sections of polystyrene particles with phosphonate groups (AZ-5VBPA). (b) ESI image of phosphorus at the same position as shown in image a. (c) Combination of the images a and b.

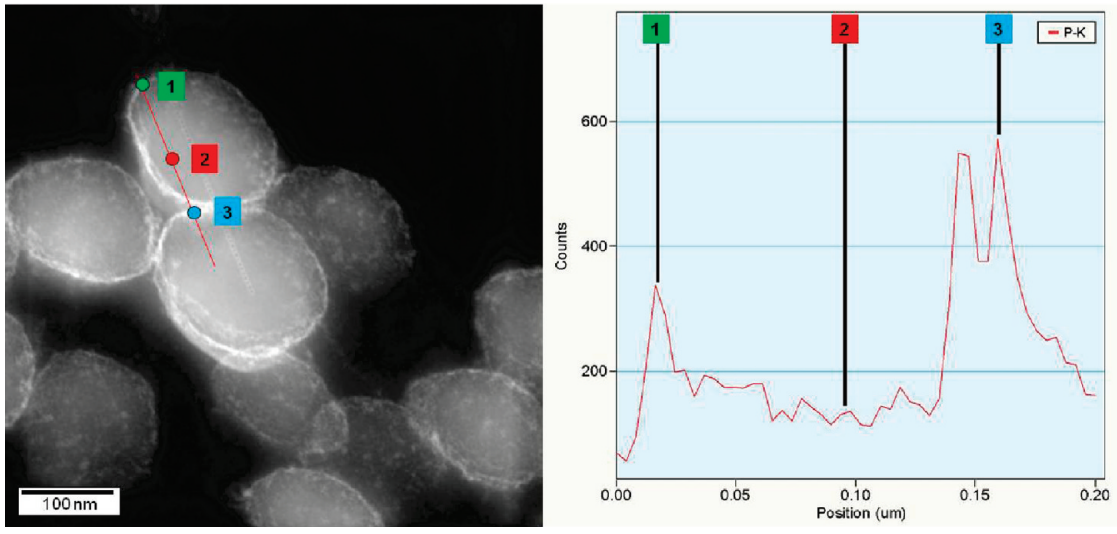

FIGURE 5. Dark-field image of polystyrene particles with phosphonate groups (AZ-5VBPA). Left image: an EDX line scan through the particle was done in the STEM mode. Positions 1 (green), 2 (red), and 3 (blue) correspond to the positions shown in the diagram (right image) that represent the phosphorus content along the EDX line.

hexagonal arrangement of the particles. To study the morphology of the particle surface, the AFM measurements were performed (Figure 7).

In the phase images, the nonfunctionalized particles show a homogeneous surface structure, whereas the phosphonated particles exhibit an inhomogeneous surface composition with two distinct phases. The existence of two phases could be due to the presence of VBPA homopolymer chains on the particle surface. The VBPA homopolymer chains are much more hydrophilic than the polystyrene because of the phosphonate groups in the side chains. Another component present during synthesis is the surfactant Lutensol AT50. However, the structure formation by the poly(ethylene glycol) chains of Lutensol AT50 as the possible cause can be excluded here because this surfactant was used during the synthesis of both types of particles.

Determination of the Adhesion Forces by AFM. To analyze the effect of the phosphonate anchor group on the interaction with metal oxide surfaces the adhesion forces between the atomic force microscope tips (AFM tips) and the particles adhered onto silicon wafer were measured. Nonfunctionalized polystyrene particles were used as a reference system. Titanium dioxide and bare silicon tip with native OH groups on their surface were used. In Figure 8 the force–distance curves recorded on polySt-polyVBPA particles (synthesized with 5 wt % VBPA, sample AZ-5VBPA) as well as pure polystyrene particles (sample AZ-0) with (a) TiO_2 tip and (b) SiO_2 tip are shown. During the AFM

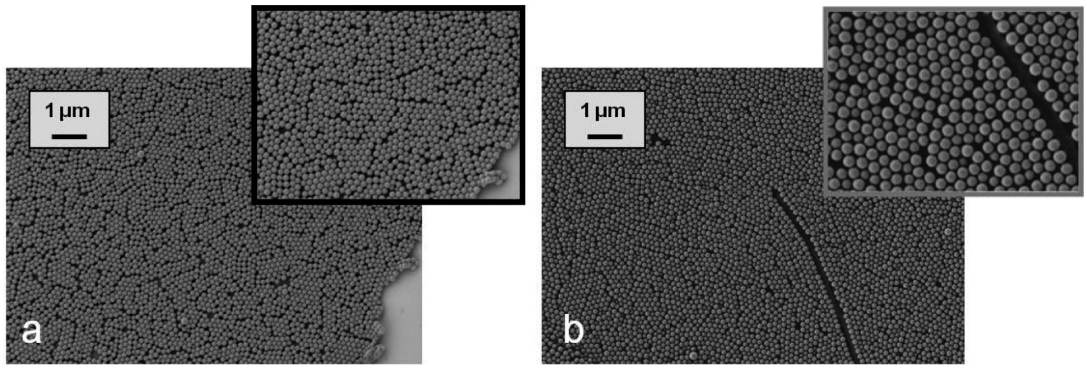

FIGURE 6. SEM images of 5 wt % polySt-polyVBPA particles (AZ-5VBPA) deposited onto (a) SiO_2 and (b) TiO_2 surfaces.

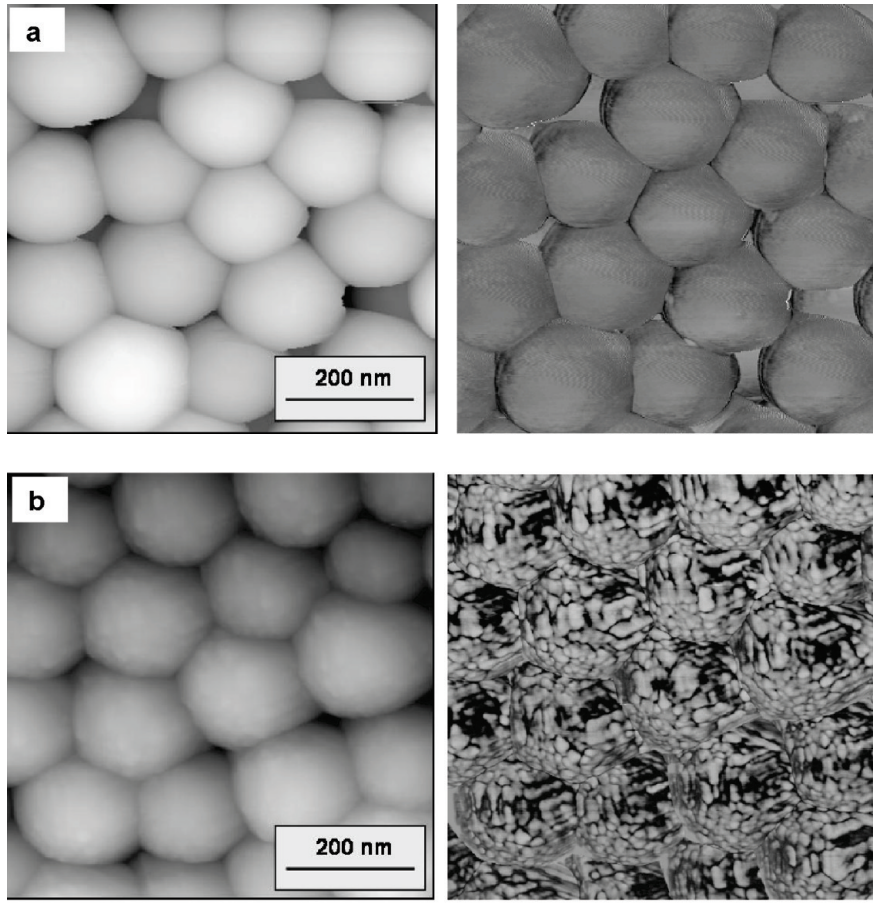

FIGURE 7. AFM height (left) and phase (right) images of (a) nonfunctionalized polystyrene particles (AZ-0) and (b) 5 wt % polySt−polyVBPA particles (AZ-5VBPA) deposited on a silicon wafer.

measurements that were performed on the same type of particles, we did not observe a big variation (or systematic decrease/increase) in the adhesion force, which might be caused by the contamination of the AFM tip. The difference in the adhesion forces within the same sample was much smaller as compared to the difference between functionalized and nonfunctionalized particles.

It can be clearly seen that the introduction of phosphonate groups leads to higher adhesion forces than in case of the nonfunctionalized particles. Table 3 summarizes the determined average adhesion forces obtained by force−distance curves measured at different positions on the particles and particle layers.

The adhesion forces between the nonfunctionalized polystyrene particles and the silicon dioxide as well as the titanium dioxide tip are approximately 13 nN independent of the tip material. The forces between the silicon dioxide tip and the phosphonated particles are significantly higher with 43.4 (±3.6) nN. The strongest adhesion forces are observed between the titanium dioxide tip and the phosphonated particles, reaching 63.9 (±4.3) nN. It can be assumed that the higher adhesion forces in the case of titanium dioxide might be due to the higher amount of hydroxyl groups that are present on the surface. According to the quantitative XPS studies performed on the native air-formed oxide films of titanium and silicon, the surface

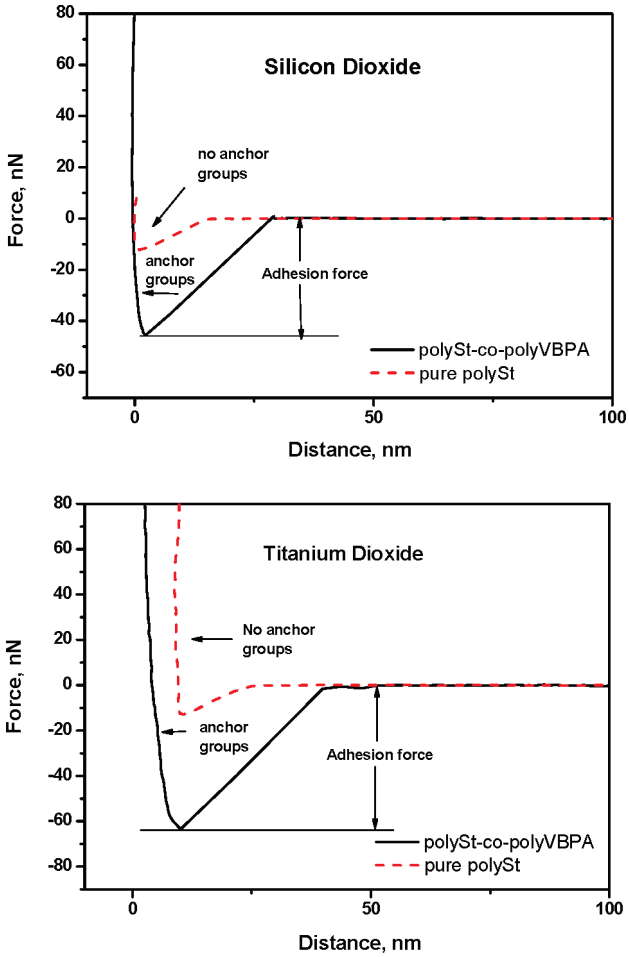

FIGURE 8. Force–distance curves of 5 wt % polySt–polyVBPA (AZ-5VBPA) and pure polystyrene particles (AZ-0) monolayer onto (a) silicon and (b) TiO_2 surfaces. Only the retract part of the force curves is shown.

Table 3. Adhesion Forces Between Pure Polystyrene Particles or Polystyrene Particles Functionalized with Phosphonate Anchor Groups and a Silicon or Titanium Dioxide AFM Tip

sample name	anchor group	tip material	adhesion force (nN)[a]
AZ-0	no anchor group	SiO_2	12.5 ± 2.6
AZ-5VBPA	$-PO_3H_2$	SiO_2	43.4 ± 3.6
AZ-0	no anchor group	TiO_2	13.4 ± 0.9
AZ-5VBPA	$-PO_3H_2$	TiO_2	63.9 ± 4.3

[a] Mean values of 100 force–distance curves on 10 different substrate positions.

concentration of OH groups was found to be about 11 and 8 OH groups per nm^2, respectively (32). The adhesion forces given in Table 3 are average values. As we can see from the phase images (Figure 4b right), the phosphonated particles exhibited two different phases on their surfaces. This inhomogeneity was also reflected by the adhesion force measurements. While the distribution of adhesion forces measured with a TiO_2 tip on a single particle shows a single peak for a pure polystyrene particles, the adhesion force distributions on a 5 wt % polySt–polyVBPA particle is bimodal (Figure 9).

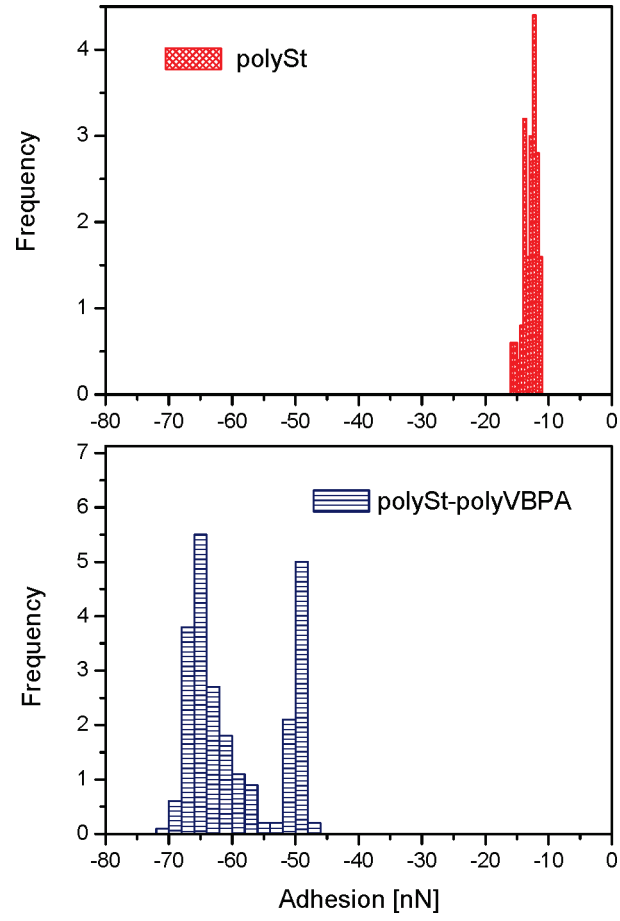

FIGURE 9. Distributions of adhesion forces between a TiO_2 tip and different locations on a single particle of (a) nonfunctionalized polystyrene (AZ-0) and (b) 5 wt % polySt–polyVBPA (AZ-5VBPA).

From Figure 9, the single curve measurement we can see that the adhesion forces for the functionalized particles are in a range from 47 to 73 nN measured with the titanium dioxide tip and in the region of 12 to 18 nN in case of the pure polystyrene particles. It can be seen that there are higher fluctuations in the adhesion forces for the phosphonated particles, because of the more inhomogeneous surface caused by the presence of VBPA homopolymer chains on the particle surface. However, in any case, the adhesion forces are much higher for the functionalized particles than for the pure polystyrene samples.

Mineralization on the Particles Adhered on the Surface. The stable formation of phosphonate-functionalized particles monolayer on titanium surface leads to an effective decoration of this material with a high density of phosphonate groups. These groups can act as nucleation sites for calcium phosphate. To demonstrate the potential of such a system for bone mineralization, the functionalized particle layer was exposed to the calcium and phosphate ions with the stoichiometric ratio of 5:3 to form hydroxyapatite. The loading was performed at the physiological temperature of 37 °C. The mineral formed on the surface of the particle can be visualized in the SEM image in Figure 10. It was found that neither the salt addition nor the stirring at 37 °C were able to disrupt the particle layer, indicating negligible influence on the particle adhesion.

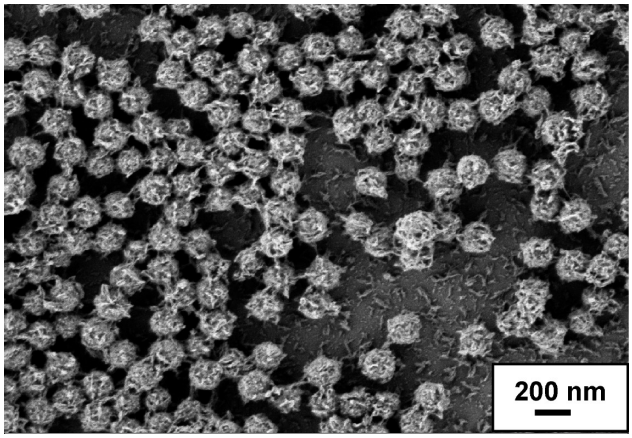

FIGURE 10. Crystal formation on the surface of polySt−polyVBPA particles (AZ-5VBPA) adhered on a silica surface.

As can be seen from the SEM image, all the particles are densely covered by the crystals proving the homogeneity of the of the crystal formation on the particle. This kind of high crystal coverage on the particle surface is similar to the previous observations with carboxyl functionalized particles dispersed in solution (25). The mineral phase formed on the particle surface is indeed hydroxyapatite was found by XRD in an analogous mineralization experiment where crystallization was performed with the VBPA functionalized particles (AZ-5VBPA) dispersed in solution.

CONCLUSIONS

Two types of polymeric nanoparticles with surface phosphonate groups were obtained via radical copolymerization of styrene with different comonomers: vinylphosponic acid (VPA) and vinylbenzyl phosphonic acid (VBPA) in miniemulsion. Particles synthesized with more hydrophobic monomers VBPA contain higher amount of surface functional groups as compared to those obtained in the presence of VPA. The TEM measurements reveal that the droplet's interface is the main locus of the copolymerization. The phosphonate functionalized particles show higher adhesion forces as compared to the nonfunctionalized particles. The adhesion forces for the functionalized particles were between 47 and 73 nN measured with the titanium dioxide tip and in the range of 12 to 18 nN in case of the pure polystyrene particles. The strong adhesion forces between the phosphonated polystyrene particles and the metal (oxide) surfaces as proven by AFM measurements make them promising candidates for the functionalization of implant surfaces. A proof of principle experiment was shown that such particle functionalized surfaces can serve as an efficient source of nucleation sites for bone mineral. By replacing polystyrene with suitable biodegradable polymers, the template particles can itself be used to release drugs or growth factors in order to treat bone defects. Hence, such functionalized particles adhered on the substrates can open new corridors in the field of tissue engineering for developing new functional implant surfaces as scaffolds for the nucleation and growth of bone mineral.

Acknowledgment. We thank Uwe Rietzler and Gabi Herrmann (MPI-P, Mainz) for their technical assistance with AFM measurements. We are also indebted to Dr. Ingo Lieberwirth, Gunnar Glasser (MPI-P, Mainz), and Reinhard Weih (University of Ulm) for their support in SEM/TEM studies and valuable discussions. This work was supported by the Baden-Württemberg Stiftung.

REFERENCES AND NOTES

(1) Busch, G.; Jaehne, E.; Cai, X. D.; Oberoi, S.; Adler, H. J. P. *Synth. Met.* **2003**, *137*, 871.
(2) Henke, A.; Jaehne, E.; Adler, H. J. P. *Macromol. Symp.* **2001**, *164*, 1.
(3) Wach, J. Y.; Malisova, B.; Bonazzi, S.; Tosatti, S.; Textor, M.; Zurcher, S.; Gademann, K. *Chem.—Eur. J.* **2008**, *14*, 10579.
(4) Khoo, X.; Hamilton, P.; O'Toole, G. A.; Snyder, B. D.; Kenan, D. J.; Grinstaff, M. W. *J. Am. Chem. Soc.* **2009**, *131*, 10992.
(5) Höök, F.; Vörös, J.; Rodahl, M.; Kurrat, R.; Böni, P.; Ramsden, J. J.; Textor, M.; Spencer, N. D.; Tengvall, P.; Gold, J. B. K. *Colloids Surf., B* **2002**, *24*, 155.
(6) Hemmersam, A. G.; Foss, M.; Chevallier, J.; F, B. *Colloids Surf., B* **2005**, *43*, 208.
(7) Kenausis, G. L.; Voros, J.; Elbert, D. L.; Huang, N. P.; Hofer, R.; Ruiz-Taylor, L.; Textor, M.; Hubbell, J. A.; ND, S. *J. Phys. Chem., B* **2000**, *104*, 3298.
(8) Siegers, C.; Biesalski, M.; Haag, R. *Chem.—Eur. J.* **2004**, *10*, 2831.
(9) Luk, Y. Y.; Kato, M.; Mrksich, M. *Langmuir* **2000**, *16*, 9604.
(10) Tosatti, S.; Michel, R.; Textor, M.; Spencer, N. D. *Langmuir* **2002**, *18*, 3537.
(11) Textor, M.; Ruiz, L.; Hofer, R.; Rossi, A.; Feldman, K.; Hahner, G.; Spencer, N. D. *Langmuir* **2000**, *16*, 3257.
(12) Mani, G.; Johnson, D. M.; Marton, D.; Feldman, M. D.; Patel, D.; Ayon, A. A.; Agrawal, C. M. *Biomaterials* **2008**, *29*, 4561.
(13) Heijink, A.; Schwartz, J.; Zobitz, M. E.; Crowder, K. N.; Lutz, G. E.; Sibonga, J. D. *Clin Orthop Relat Res* **2008**, *466*, 977.
(14) Hanson, E. L.; Schwartz, J.; Nickel, B.; Koch, N.; Danisman, M. F. *J. Am. Chem. Soc.* **2003**, *125*, 16074.
(15) Park, H.; Bae, E.; Lee, J. J.; Park, J.; Choi, W. *J. Phys. Chem. B* **2006**, *110*, 8740.
(16) Bae, E. Y.; Choi, W. Y.; Park, J. W.; Shin, H. S.; Kim, S. B.; Lee, J. S. *J. Phys. Chem. B* **2004**, *108*, 14093.
(17) Luschtinetz, R.; Oliveira, A. F.; Frenzel, J.; Joswig, J. O.; Seifert, G.; Duarte, H. A. *Surf. Sci.* **2008**, *602*, 1347.
(18) Rivas, B. L.; Pereira, E. *Macromol. Symp.* **2003**, *193*, 237.
(19) Yim, C. T.; Pawsey, S.; Morin, F. G.; Reven, L. *J. Phys. Chem., B* **2002**, *106*, 1728.
(20) Pawsey, S.; Yach, K.; Reven, L. *Langmuir* **2002**, *18*, 5205.
(21) Viornery, C.; Chevolot, Y.; Leonard, D.; Aronsson, B. O.; Pechy, P.; Mathieu, H. J.; Descouts, P.; Gratzel, M. *Langmuir* **2002**, *18*, 2582.
(22) Landfester, K. *Macromol. Rapid Commun.* **2001**, *22*, 896.
(23) Musyanovych, A.; Rossmanith, R.; Tontsch, C.; Landfester, K. *Langmuir* **2007**, *23*, 5367.
(24) Ziegler, A.; Landfester, K.; Musyanovych, A. *Colloid Polym. Sci.* **2009**, *287*, 1261.
(25) Ethirajan, A.; Ziener, U.; Landfester, K. *Chem. Mater.* **2009**, *21*, 2218.
(26) Wyman, P.; Crook, V.; Hunt, B. J.; Ebdon, J. *Des. Monomers Polym.* **2004**, *7*, 301.
(27) Hutter, J. L.; Bechhoefer, J. *Rev. Sci. Instrum.* **1993**, *64*, 1868.
(28) Butt, H.-J.; Kappl, M. *Adv. Colloid Interface Sci.* **2009**, *146*, 48.
(29) Landfester, K.; Eisenblatter, J.; Rothe, R. *J. Coat. Technol. Res.* **2004**, *1*, 65.
(30) Marinova, K. G.; Alargova, R. G.; Denkov, N. D.; Velev, O. D.; Petsev, D. N.; Ivanov, I. B.; Borwankar, R. P. *Langmuir* **1996**, *12*, 2045.
(31) Geyer, G. *Ultrahistochemie*; 2nd ed.; VEB G. Fischer-Verlag: Jena, Germany, 1972.
(32) McCafferty, E.; Wightman, J. P. *Surf. Interface Anal.* **1998**, *26*, 549.

AM1004305